nature medicine

# A chronic low dose of $\Delta^9$-tetrahydrocannabinol (THC) restores cognitive function in old mice

Andras Bilkei-Gorzo[1,4], Onder Albayram[1,4], Astrid Draffehn[2], Kerstin Michel[1], Anastasia Piyanova[1], Hannah Oppenheimer[3], Mona Dvir-Ginzberg[3], Ildiko Rácz[1], Thomas Ulas[2], Sophie Imbeault[1], Itai Bab[3], Joachim L Schultze[2] & Andreas Zimmer[1]

© 2017 Nature America, Inc., part of Springer Nature. All rights reserved.

**The balance between detrimental, pro-aging, often stochastic processes and counteracting homeostatic mechanisms largely determines the progression of aging. There is substantial evidence suggesting that the endocannabinoid system (ECS) is part of the latter system because it modulates the physiological processes underlying aging[1,2]. The activity of the ECS declines during aging, as CB1 receptor expression and coupling to G proteins are reduced in the brain tissues of older animals[3–5] and the levels of the major endocannabinoid 2-arachidonoylglycerol (2-AG) are lower[6]. However, a direct link between endocannabinoid tone and aging symptoms has not been demonstrated. Here we show that a low dose of $\Delta^9$-tetrahydrocannabinol (THC) reversed the age-related decline in cognitive performance of mice aged 12 and 18 months. This behavioral effect was accompanied by enhanced expression of synaptic marker proteins and increased hippocampal spine density. THC treatment restored hippocampal gene transcription patterns such that the expression profiles of THC-treated mice aged 12 months closely resembled those of THC-free animals aged 2 months. The transcriptional effects of THC were critically dependent on glutamatergic CB1 receptors and histone acetylation, as their inhibition blocked the beneficial effects of THC. Thus, restoration of CB1 signaling in old individuals could be an effective strategy to treat age-related cognitive impairments.**

To determine whether prolonged exposure to a low dose of THC has lasting effects on learning and memory performance in mice aged 2, 12 and 18 months (termed young, mature and old, respectively), we implanted osmotic minipumps releasing 3 mg per kg bodyweight per day of THC or vehicle for 28 d. The effects of age and treatment on spatial learning and memory were first assessed in the Morris water maze (MWM) test starting on day 33 after pump implantation, thus allowing a washout period of 5 d (**Fig. 1a**). The mature and old vehicle-treated animals learned the task more slowly than the young animals, which is indicative of an age-related deficit in spatial learning (**Fig. 1b**). Treatment with THC improved task acquisition in mature and old animals. The difference between the groups persisted in the reversal phase of the test, which assessed learning flexibility. Thus, both THC-treated mature and old mice showed better performance than the vehicle-treated controls in the same age groups. In the probe trial phase of the test, which was conducted on day 6 before reversal learning and which is an indicator of long-term spatial memory, vehicle-treated old animals showed memory impairments, as indicated by reduced time spent in the target quadrant (**Fig. 1c**). Treatment with THC improved spatial memory in this age group to the level observed with the young controls. In young mice, THC treatment worsened performance, in good agreement with the known detrimental effects of THC on cognition in young animals and humans[7–9]. Treatment with THC did not affect the time the mice required to reach a visible platform (**Supplementary Fig. 1a**).

We next used the novel object location recognition task. Young, vehicle-treated controls performed significantly better than vehicle-treated mature and old animals (**Fig. 1d**), which again indicates an age-related impairment of cognitive performance. THC treatment also abolished the cognitive deficit in mature and old animals in this test, as they performed at the same level as the young, vehicle-treated controls. THC treatment was already effective in mature animals after 14 d (**Supplementary Fig. 1b**). To further test the effect of THC treatment on long-term memory, animals were tested in the partner recognition test. Here the test mouse first explores an open-field arena with an unknown conspecific in a small grid cage and a small object. This test was repeated after 24 h with a new partner in an identical grid cage instead of the object. If mice remember the previous partner from session 1, they will show a higher preference for the new partner. Mature and old animals did not remember the partner as well as young mice (**Fig. 1e**), but THC treatment restored partner-recognition ability in mature and old animals (**Supplementary Fig. 1c**). Together, these results reveal a profound, long-lasting improvement of cognitive performance resulting from a low dose of THC treatment in mature and old animals. THC treatment for 28 d restored the learning and memory performance of mature and old animals in the MWM, novel object location recognition and social recognition tests to the levels observed in young mice.

[1]Institute of Molecular Psychiatry, University of Bonn, Bonn, Germany. [2]Genomics and Immunoregulation, LIMES Institute, Bonn, Germany. [3]Institute of Dental Sciences, Hebrew University, Jerusalem, Israel. [4]These authors contributed equally to this work. Correspondence should be addressed to A.Z. (neuro@uni-bonn.de).

Received 27 July 2015; accepted 7 February 2017; published online 8 May 2017; doi:10.1038/nm.4311

© 2017 Nature America, Inc., part of Springer Nature. All rights reserved.

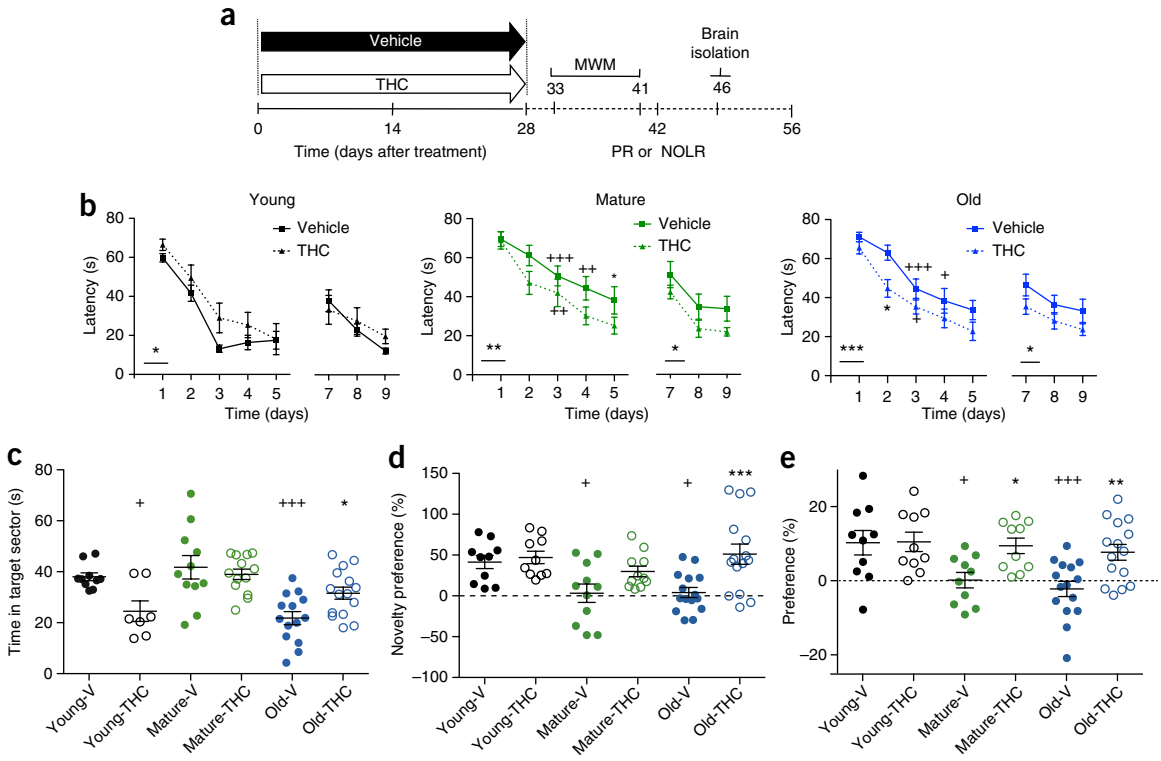



**Figure 1** Chronic, low-dose THC treatment restores learning ability in aged mice. (**a**) Experimental setup used for assessing the long-lasting behavioral and cellular responses to chronic THC administration. PR, partner recognition; NOLR, novel object location recognition. (**b**) Acquisition and reversal phases of the Morris water maze (MWM) in vehicle (V)- or THC-treated mice aged 2 months (young), 12 months (mature) and 18 months (old). Shorter escape latencies are indicative of better learning and memory performance. Young-V, $n = 10$; young-THC, $n = 7$; mature-V and mature-THC, $n = 11$; old-V, $n = 14$; old-THC, $n = 15$ mice. Asterisks above the horizontal bars indicate significant main treatment effects: $^{*}P < 0.05$, $^{**}P < 0.01$, $^{***}P < 0.0001$, two-way ANOVA. (**c**) Probe trial phase of the MWM, which assessed long-term memory. A longer time in the target sector is indicative of better memory performance. Young-V, $n = 10$; young-THC, $n = 7$; mature-V, $n = 11$; mature-THC, $n = 13$; old-V, $n = 14$; old-THC, $n = 15$. (**d**) Effect of THC on novel object location recognition memory. Preference for the object in a new position (novelty preference) is an indicator that animals have recognized the repositioning of the object. The dashed line indicates the chance level. Young, $n = 10$; mature, $n = 11$; old, $n = 15$. (**e**) Results of the partner-recognition test. Preference for a new partner indicates partner recognition. The dashed line indicates the chance level. Young, $n = 10$; mature, $n = 10$; old, $n = 15$. $^{*}P < 0.05$, $^{**}P < 0.01$, $^{***}P < 0.001$, significant difference when compared to vehicle-treated mice; $^{+}P < 0.05$, $^{++}P < 0.01$, $^{+++}P < 0.001$, significant difference when compared to vehicle-treated young mice. Statistical significance was calculated using two-way ANOVA in **b** and one-way ANOVA in **c**–**e**, followed by Bonferroni's *t*-test. In (**c**–**e**), circles represent data from individual animals. Means and s.e.m. are shown. See also **Supplementary Figure 1** and **Supplementary Table 4**.

We next investigated the effect of THC on synaptic density in the hippocampus. Expression of the synaptic marker proteins synapsin I, synaptophysin and postsynaptic density protein 95 (PSD95) was lower in mature animals than in young ones (**Fig. 2a**), which is indicative of an age-related loss of synaptic connectivity[10,11]. THC treatment did not alter the expression of these proteins in young mice, but it increased the synapsin I and synaptophysin levels of mature animals to those observed in young, THC-free mice. These results were confirmed by immunohistochemistry (**Supplementary Fig. 2**). Further experiments showed that THC increased hippocampal spine density and affected the balance of inhibitory versus excitatory synapses (**Supplementary Results** and **Supplementary Fig. 2**). We next established gene expression profiles in the whole hippocampus 50 d after minipump implantation. A total of 21,198 transcripts were identified. Hierarchical clustering of variably expressed genes ($P < 0.05$, $n = 2{,}090$ genes) within the data set clearly revealed a four-group structure based on treatment and age (**Fig. 2b** and **Supplementary Fig. 3**). Most strikingly, THC-treated mature animals closely resembled vehicle-treated young mice, while THC treatment of young mice resulted in a gene expression pattern more similar to that of vehicle-treated mature animals. Using the two-way ANOVA model ($P < 0.05$, fold change = 1.5), we identified 100 transcripts differentially regulated by THC in young mice and 232 in mature mice (**Supplementary Fig. 3**). Of these, only 13 overlapped (**Supplementary Fig. 4**). Gene ontology enrichment analysis (GOEA) followed by network visualization comparing the vehicle- and THC-treated old groups (**Fig. 2c**) identified large clusters of gene ontology (GO) terms associated with morphogenesis, homeostasis, gene expression, phosphorylation and nerve impulse transmission. This result indicates that THC treatment affects molecular processes relevant to cell plasticity and signaling in mature animals. Upregulated transcripts included Klotho (*Kl*) (**Fig. 2d** and **Supplementary Figs. 5** and **6**), which is known to extend lifespan in different species[12–14] and to improve cognition[15]; transthyretin (*Ttr*), a gene that is thought to be protective against Alzheimer's disease[16,17]; and brain-derived neurotrophic factor (*Bdnf*), an important neurotrophic factor that enhances synapse formation[18] and cognitive functions[19,20]. The two transcripts that were most strongly downregulated in the mice after THC treatment corresponded to genes with potential pro-aging effects: caspase-1 (*Casp1*), which is involved in age-related impairments in cognition[21], and connective tissue growth factor (*Ctgf*), which is known to enhance the pro-apoptotic activity of transforming growth factor β (TGF-β)[22] (**Supplementary Fig. 7**). Together, these results demonstrate that the cognitive improvements in THC-treated mature mice were associated

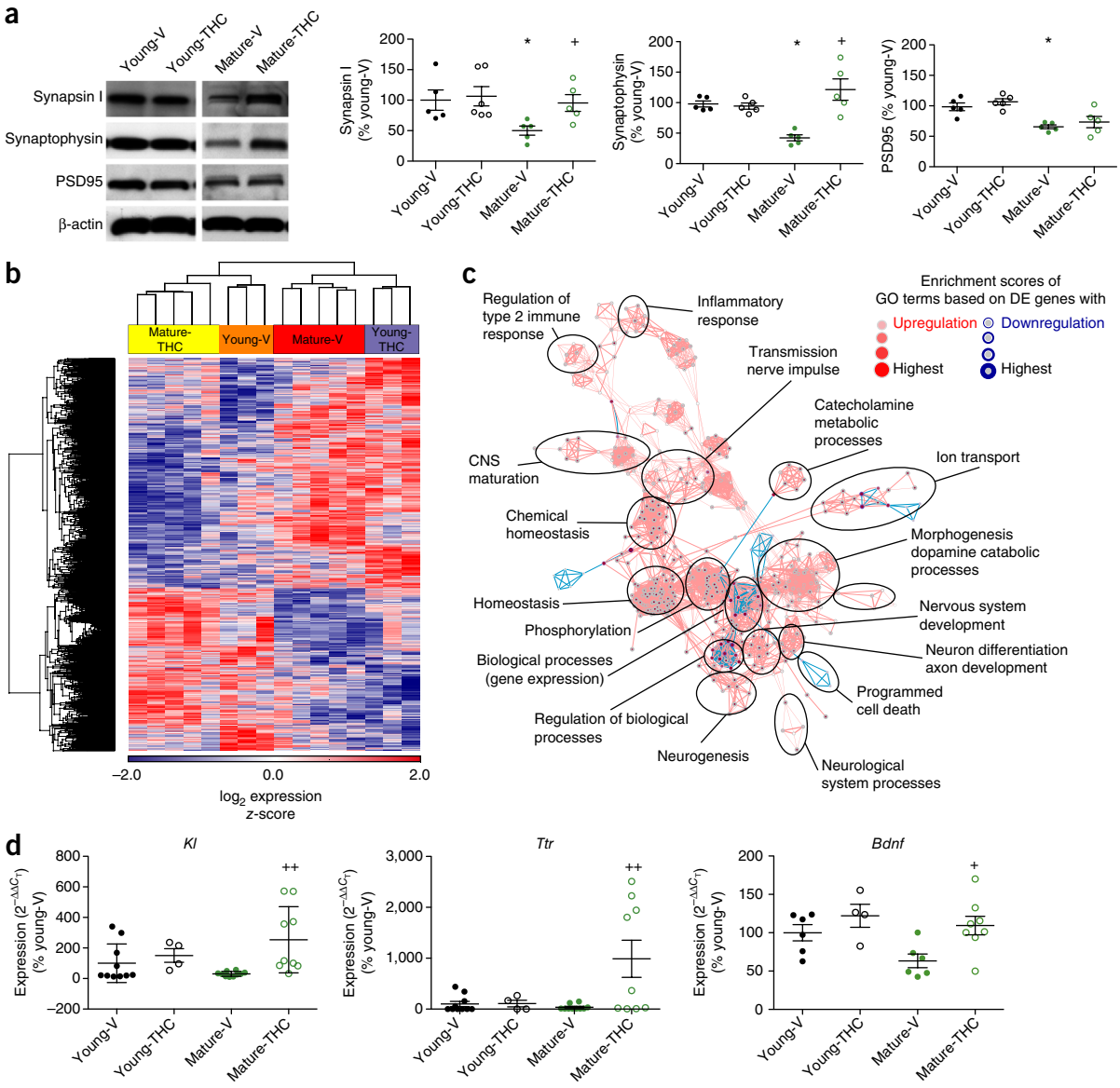



**Figure 2** Molecular changes in the hippocampus induced by low-dose THC treatment. (**a**) Representative immunoblots and quantification of the synaptic proteins synapsin I, synaptophysin and PSD95 from the hippocampal lysates of young and mature mice 22 d after termination of the treatments. $n = 5$ mice for all groups, except for young-THC at synapsin I, where $n = 6$. $^{*}P < 0.05$, difference between young-V and mature-V; $^{+}P < 0.05$, difference between mature-V and mature-THC. Significance was calculated using one-way ANOVA followed by Bonferroni's *t*-test. (**b**) Hierarchical clustering of 2,090 variably expressed genes shown as *z*-transformed $\log_2$ expression values (ANOVA, $P \leq 0.05$). (**c**) Network visualization of gene ontology enrichment analysis based on the 156 most upregulated and 76 most downregulated transcripts between the mature-THC and mature-V groups using BiNGO and EnrichmentMap. Enriched GO terms based on upregulated transcripts are depicted as red nodes and enriched GO terms based on downregulated transcripts are represented as blue nodes, where node color and size represent the corresponding false discovery rate (FDR)-adjusted enrichment *P* value (*Q* value). DE, differentially expressed. (**d**) Expression of Klotho (*Kl*), transthyretin (*Ttr*) and *Bdnf* using an independent set of animals as assessed by quantitative real-time PCR. *Kl* and *Ttr*: young-V and mature-V, $n = 10$; young-THC, $n = 4$; mature-THC, $n = 9$. Bdnf: young-V and mature-V, $n = 6$; young-THC, $n = 4$; mature-THC, $n = 8$. $^{++}P < 0.01$, difference between mature-V and mature-THC mice. Significance was calculated using one-way ANOVA followed by Bonferroni's *t*-test. In **a** and **d**, circles represent data from individual animals. Means and s.e.m. are shown. See also **Supplementary Figures 2–7** and **10**, **Supplementary Data**, and **Supplementary Tables 1** and **2**.

with a change in gene profiles; these changes and the associated cognitive improvements both lasted for several weeks after cessation of the treatment. The directions of the expression changes were such that the profiles of mature, THC-treated mice were most similar to those of young control mice, whereas THC treatment of young mice resulted in a gene expression pattern that was similar to that of vehicle-treated mature animals. This indicates that the enhanced CB1 tone achieved through low-dose THC treatment may have normalized the weak cannabinoid signaling signature in mature animals and thus reverted some of the age-related changes in gene expression, whereby several genes with antiaging effects were upregulated while genes contributing to aging were downregulated. The opposite transcriptional changes with THC treatment in young animals are interesting and deserve further investigation.

THC, similar to other drugs of abuse[23], can activate cAMP-response-element-binding protein (CREB)[24,25], a molecular switch that converts short-term, plastic changes into long-lasting adaptations[26], thus playing

© 2017 Nature America, Inc., part of Springer Nature. All rights reserved.

a key role in learning and memory[27]. Increased CREB signaling is involved in the memory-promoting effect of young blood in models of parabiosis[28] and caloric restriction[29]. THC can induce long-term changes in neuronal activity directly by the activation of genes with CREB-inducible promoter regions and indirectly through epigenetic changes induced by recruiting CREB-binding protein (CBP), a histone acetyltransferase

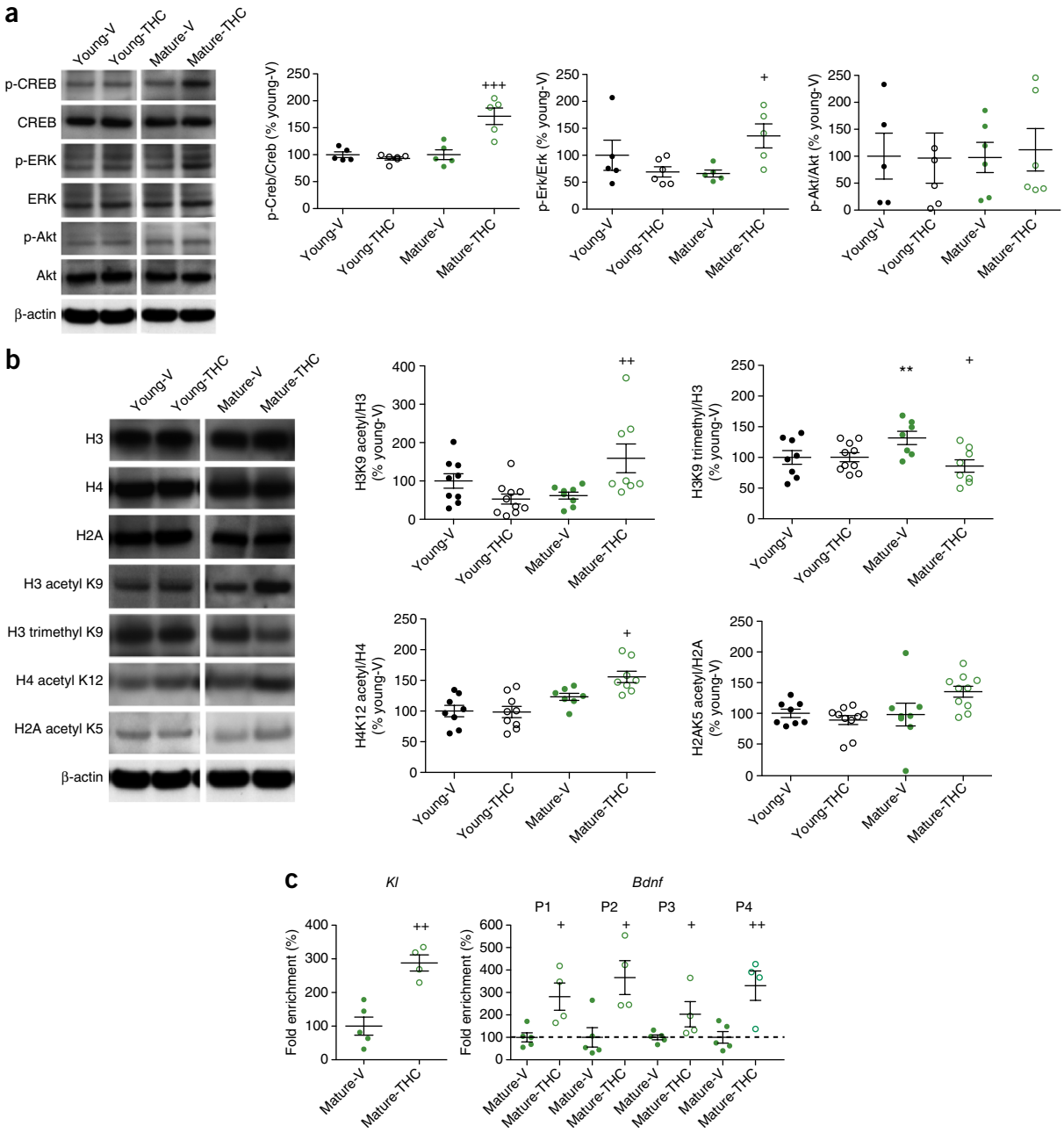



**Figure 3** Epigenetic changes induced by low-dose THC treatment in hippocampal tissue. (**a**) Representative immunoblots of phosphorylated and total cAMP-response-element-binding protein (CREB), extracellular-signal-regulated kinases 1/2 (Erk1/2) and thymoma viral proto-oncogene (Akt) proteins from hippocampal lysates and quantitative analysis of the phosphorylation state of CREB, Erk1/2 and Akt. Young-V, mature-V and mature-THC, $n = 5$; young-THC, $n = 6$ mice, except for the pAkt/Akt panel, where mature-V and mature-THC, $n = 6$; young-THC, $n = 5$. (**b**) Representative immunoblots and quantitative analysis of global changes in the total levels of histone H3, H4 and H2A proteins, as well as different acetylated and trimethylated forms, from hippocampal lysates. Band intensities for modified histones were normalized to those for the respective histone. H3 acetyl K9/H3: young-V, $n = 9$; mature-V and mature-THC, $n = 8$; young-THC, $n = 10$; H3 trimethyl K9/H3: young-V and mature-THC, $n = 8$; mature-V, $n = 7$; young-THC, $n = 10$; H4 acetyl K12/H4: young-V and mature-THC, $n = 8$; mature-V, $n = 7$; young-THC, $n = 9$; H2A acetyl K5/H2A: young-V and mature-V, $n = 8$; mature-THC and young-THC, $n = 10$. (**c**) AcH3K9 enrichment was analyzed at the promoter regions of *KI* and *Bdnf* by ChIP assays in the hippocampus of mature-V ($n = 5$) and mature-THC ($n = 4$) mice. $^{*}P < 0.05$, $^{**}P < 0.01$, difference between young-V and mature-V; $^{+}P < 0.05$, $^{++}P < 0.01$, $^{+++}P < 0.001$, difference between mature-V and mature-THC. One-way ANOVA followed by Bonferroni's *t*-test was used to calculate significance in immunoblotting, and Student's *t*-test was used for the ChIP analysis. Circles represent data from individual mice. P1, P2, P3,and P4 denote the four promoter regions of *Bdnf*. Vehicle controls were adjusted to 100%, as indicated by the dashed line. Means and s.e.m. are shown. See also **Supplementary Figure 8**, **Supplementary Data**, and **Supplementary Table 3**.

© 2017 Nature America, Inc., part of Springer Nature. All rights reserved.

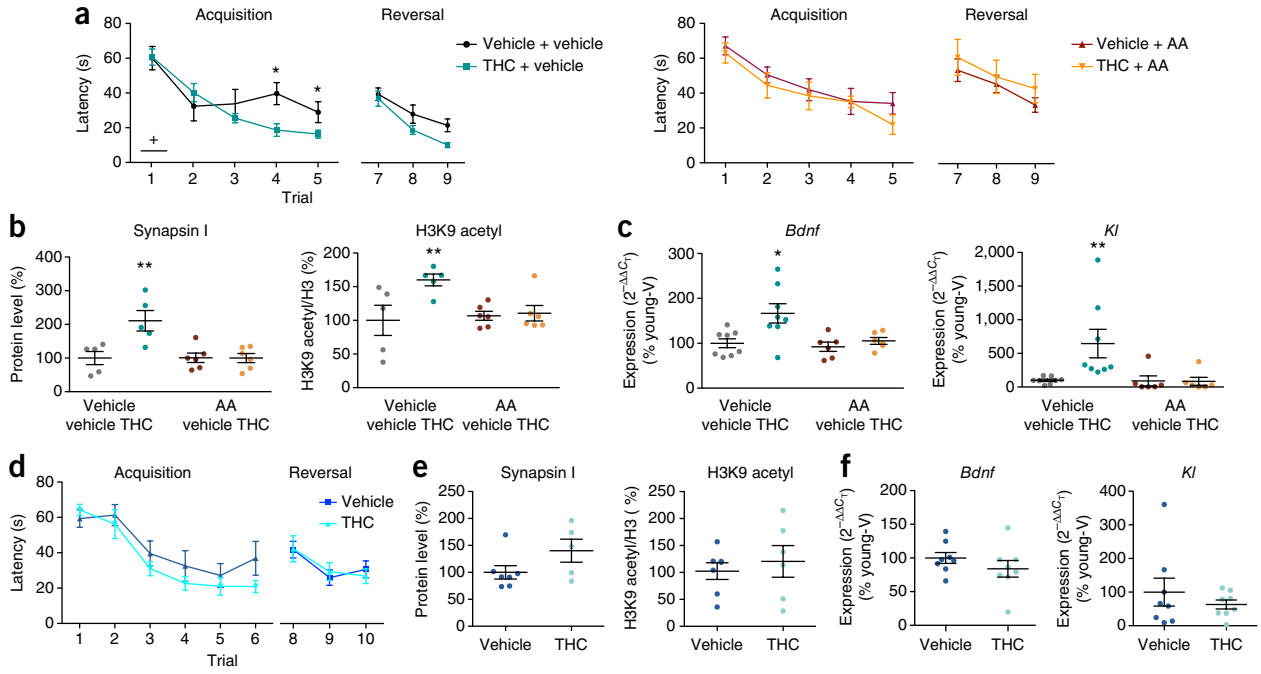



**Figure 4** The effects of low-dose THC treatment in mature animals are blocked by the histone acetyltransferase inhibitor anacardic acid and are absent in mice with deletion of *Cb1* in glutamatergic neurons. (**a**) Spatial learning and memory in the MWM test using THC- and vehicle-treated mature animals with or without AA treatment. Vehicle + vehicle and THC + AA, $n = 7$; THC + vehicle, $n = 8$; vehicle + AA, $n = 9$. $^{+}P < 0.05$, significant treatment effect as determined by two-way ANOVA; $^{*}P < 0.05$, significant difference between vehicle- and THC-treated mice as determined by Bonferroni's *post hoc* test. (**b**) Quantification of synapsin I protein levels and acetylation of histone H3. Vehicle groups, $n = 5$; AA groups, $n = 6$. (**c**) *Bdnf* and *Kl* transcription in mice aged 12 months. Vehicle groups, $n = 8$; AA groups, $n = 6$. (**d**) Effect of THC treatment on MWM test performance in *Neurod6-Cre*; *Cb1*$^{-/-}$ mice aged 12 months. Vehicle group, $n = 8$; THC group, $n = 7$. (**e**) Effect of THC treatment on synapsin I protein levels and H3K9 acetylation (vehicle group, $n = 7$; THC group, $n = 6$, except for synapsin I, where $n = 5$). (**f**) *Bdnf* and *Kl* expression ($n = 8$ for both groups) of *Neurod6-Cre*; *Cb1*$^{-/-}$ mice aged 12 months. In **b**–**f**, vehicle controls are set at 100%. $^{*}P < 0.05$, $^{**}P < 0.01$, one-way ANOVA followed by Bonferroni's *t*-test. Circles represent data from individual mice. Means and s.e.m. are shown. See also **Supplementary Figures 9** and **10**, **Supplementary Data**, and **Supplementary Table 4**.

that is specific for histones H3 and H4. To investigate whether these mechanisms contributed to the effects of chronic THC treatment, we analyzed CREB signaling, as well as the CB1-downstream Akt and extracellular-signal-regulated kinase (Erk) pathways. THC treatment significantly increased Erk1 and Erk2 (Erk1/2) and CREB phosphorylation in mature animals but not in young ones (**Fig. 3a**)[30], whereas phosphorylation of Akt was not different between groups. Activated CREB stimulates transcription of several genes that modulate synaptic plasticity, including *Bdnf*[31], and recruits the histone acetyltransferase CBP (p300)[32]. CBP facilitates acetylation of H3 and H4 histones, thus transforming chromatin into a relaxed configuration and making it more accessible to transcription factors[33]. The levels of acetylated H3K9 and H4K12 were significantly elevated (+60.0% and +22.9%, respectively) in the hippocampus of THC-treated mature animals in comparison to control animals from the same age group, with these increases already visible after 14 d of THC treatment (**Supplementary Fig. 8**), whereas trimethylation of H3K9 was decreased (**Fig. 3b**). AcH2A, which is not regulated by CBP, remained unchanged after THC treatment. AcH3K9 was also markedly increased at the *Kl* promoter and at all four *Bdnf* promoters, as revealed by chromatin immunoprecipitation (ChIP) analysis (**Fig. 3c**). This may suggest that the increased expression of *Bdnf* and possibly other CBP-regulated genes is caused by THC-induced epigenetic changes. BDNF is an upstream activator and *Bdnf* is a major downstream target of CREB-mediated signaling[34]. Expression of *Bdnf* and *Ntrk2* (*TrkB*) decreases during aging[35]. Our results are consistent with such a CBP-mediated mechanism and with the demonstration that histone acetylation promotes cognitive functions, whereas the opposing process, histone deacetylation, negatively affects cognition[36].

To directly test this hypothesis, a histone acetyltransferase inhibitor, anacardic acid (AA), was administered intraperitoneally on a daily basis to a new cohort of mature mice carrying osmotic minipumps releasing either vehicle or THC. AA treatment alone did not affect animal performance in the MWM (**Supplementary Table 4**), but it completely blocked the THC-induced improvement of cognitive functions (**Fig. 4a**). It also abolished the THC-induced increase in AcH3K9, the increased expression of synapsin I (**Fig. 4b**), the increase in *Bdnf* and *Kl* mRNA expression (**Fig. 4c**), and the decrease in *Casp1* or *Ctgf* expression (**Supplementary Fig. 9**). These data demonstrate that the beneficial effects of low-dose THC administration are dependent on an epigenetic mechanism involving histone acetylation. This is in line with previous findings showing that enhanced histone acetylation can result in recovery of cognitive abilities in old mice[37].

We finally asked to what extent the effects of THC are mediated by the CB1 receptor. Disrupted CB1 signaling in *Cb1*$^{-/-}$ (*Cnr1*$^{-/-}$) mice initially leads to superior learning and memory performance at a young age, but then to a rapid decline in cognitive abilities. *Cb1*$^{-/-}$ mice aged 5 months already show striking impairments in a broad range of memory models[38] accompanied by typical histological and molecular markers of old age, such as loss of hippocampal neurons, increased inflammation markers[39] and disrupted proteostasis[40]. When THC or vehicle was infused from minipumps into mature *Cb1*$^{-/-}$ mice, it had no effect on their behavior in the MWM

© 2017 Nature America, Inc., part of Springer Nature. All rights reserved.

and did not influence gene expression, synapsin I densities or histone acetylation (**Supplementary Fig. 10**), thus indicating that the beneficial effects of THC are dependent on CB1 signaling. Furthermore, we also treated mice lacking CB1 on forebrain glutamatergic principal neurons, *Neurod6-Cre*; *Cb1*$^{-/-}$ mice, which show no age-related phenotypes[41]. In these animals, THC administration also had no effect on the acquisition or reversal phase in the MWM test (**Fig. 4d**), and it did not change synapsin I protein levels, AcH3K9 (**Fig. 4e**), or the mRNA levels of *Bdnf* and *Kl* (**Fig. 4f**), *Casp1* or *Ctgf* (**Supplementary Fig. 10f**). Thus, the effects of THC on cognitive performance, synaptogenesis, histone acetylation and the expression of age-related genes were all dependent on the CB1 signaling of forebrain glutamatergic neurons. The results do not exclude the possibility that CB1 receptors on other neurons are also involved.

Attempts to reverse age-related epigenetic processes through a pharmacological blockade of histone deacetylases have shown some promise in rodents[33,42], but the deleterious side-effects have prevented application in humans[43]. Consequently, the generalized inhibition of histone deacetylation is not further considered to be a suitable treatment of age-related pathologies. In contrast, cannabis preparations and THC are used for medicinal purposes. They have an excellent safety record and do not produce adverse side-effects when administered at a low dose to older individuals. Thus, chronic, low-dose treatment with THC or cannabis extracts could be a potential strategy to slow down or even to reverse cognitive decline in the elderly.

## METHODS

Methods, including statements of data availability and any associated accession codes and references, are available in the online version of the paper.

*Note: Any Supplementary Information and Source Data files are available in the online version of the paper.*


### ACKNOWLEDGMENTS

This work was supported by the Deutsche Forschungsgemeinschaft grants FOR926 (SP2 and CP2), BI-1227/5 and SFB645. J.L.S. and A.Z. are members of the DFG Cluster of Excellence ImmunoSensation.


### AUTHOR CONTRIBUTIONS

O.A., A.B.-G., J.L.S., M.D.-G., I.B. and A.Z. designed research; O.A., A.P., S.I., T.U., H.O., I.R., K.M., A.D. and A.B.-G. performed research; O.A., A.P., A.B.-G., T.U., J.L.S. and A.Z. analyzed data; and O.A., A.B.-G., J.L.S. and A.Z. wrote the paper.

### COMPETING FINANCIAL INTERESTS

The authors declare no competing financial interests.

Reprints and permissions information is available online at http://www.nature.com/reprints/index.html.


1. Di Marzo, V., Stella, N. & Zimmer, A. Endocannabinoid signalling and the deteriorating brain. *Nat. Rev. Neurosci.* **16**, 30–42 (2015).
2. Bilkei-Gorzo, A. The endocannabinoid system in normal and pathological brain ageing. *Phil. Trans. R. Soc. Lond. B* **367**, 3326–3341 (2012).
3. Wang, L., Liu, J., Harvey-White, J., Zimmer, A. & Kunos, G. Endocannabinoid signaling via cannabinoid receptor 1 is involved in ethanol preference and its age-dependent decline in mice. *Proc. Natl. Acad. Sci. USA* **100**, 1393–1398 (2003).
4. Berrendero, F. *et al.* Changes in cannabinoid receptor binding and mRNA levels in several brain regions of aged rats. *Biochim. Biophys. Acta* **1407**, 205–214 (1998).
5. Romero, J. *et al.* Loss of cannabinoid receptor binding and messenger RNA levels and cannabinoid agonist–stimulated [$^{35}$S]guanylyl-5′*O*-(thio)-triphosphate binding in the basal ganglia of aged rats. *Neuroscience* **84**, 1075–1083 (1998).
6. Piyanova, A. *et al.* Age-related changes in the endocannabinoid system in the mouse hippocampus. *Mech. Ageing Dev.* **150**, 55–64 (2015).
7. Han, J. *et al.* Acute cannabinoids impair working memory through astroglial CB1 receptor modulation of hippocampal LTD. *Cell* **148**, 1039–1050 (2012).
8. Puighermanal, E., Busquets-Garcia, A., Maldonado, R. & Ozaita, A. Cellular and intracellular mechanisms involved in the cognitive impairment of cannabinoids. *Phil. Trans. R. Soc. Lond. B* **367**, 3254–3263 (2012).
9. Varvel, S.A., Anum, E., Niyuhire, F., Wise, L.E. & Lichtman, A.H. $\Delta^9$-THC-induced cognitive deficits in mice are reversed by the $GABA_A$ antagonist bicuculline. *Psychopharmacology (Berl.)* **178**, 317–327 (2005).
10. Head, E. *et al.* Synaptic proteins, neuropathology and cognitive status in the oldest-old. *Neurobiol. Aging* **30**, 1125–1134 (2009).
11. Morrison, J.H. & Baxter, M.G. The ageing cortical synapse: hallmarks and implications for cognitive decline. *Nat. Rev. Neurosci.* **13**, 240–250 (2012).
12. Duce, J.A. *et al.* Gene profile analysis implicates Klotho as an important contributor to aging changes in brain white matter of the rhesus monkey. *Glia* **56**, 106–117 (2008).
13. Kurosu, H. *et al.* Suppression of aging in mice by the hormone Klotho. *Science* **309**, 1829–1833 (2005).
14. Semba, R.D. *et al.* Plasma klotho and mortality risk in older community-dwelling adults. *J. Gerontol. A Biol. Sci. Med. Sci.* **66**, 794–800 (2011).
15. Dubal, D.B. *et al.* Life extension factor klotho enhances cognition. *Cell Rep.* **7**, 1065–1076 (2014).
16. Cuenco, K.T. *et al.* Association of *TTR* polymorphisms with hippocampal atrophy in Alzheimer disease families. *Neurobiol. Aging* **32**, 249–256 (2011).
17. Li, X. & Buxbaum, J.N. Transthyretin and the brain re-visited: is neuronal synthesis of transthyretin protective in Alzheimer's disease? *Mol. Neurodegener.* **6**, 79 (2011).
18. Tanaka, J. *et al.* Protein synthesis and neurotrophin-dependent structural plasticity of single dendritic spines. *Science* **319**, 1683–1687 (2008).
19. Neidl, R. *et al.* Late-life environmental enrichment induces acetylation events and nuclear factor κB–dependent regulations in the hippocampus of aged rats showing improved plasticity and learning. *J. Neurosci.* **36**, 4351–4361 (2016).
20. Erickson, K.I. *et al.* Exercise training increases size of hippocampus and improves memory. *Proc. Natl. Acad. Sci. USA* **108**, 3017–3022 (2011).
21. Gemma, C. & Bickford, P.C. Interleukin-1β and caspase-1: players in the regulation of age-related cognitive dysfunction. *Rev. Neurosci.* **18**, 137–148 (2007).
22. Khodosevich, K. *et al.* Connective tissue growth factor regulates interneuron survival and information processing in the olfactory bulb. *Neuron* **79**, 1136–1151 (2013).
23. Robison, A.J. & Nestler, E.J. Transcriptional and epigenetic mechanisms of addiction. *Nat. Rev. Neurosci.* **12**, 623–637 (2011).
24. Derkinderen, P. *et al.* Regulation of extracellular signal–regulated kinase by cannabinoids in hippocampus. *J. Neurosci.* **23**, 2371–2382 (2003).
25. Valjent, E. *et al.* $\Delta^9$-tetrahydrocannabinol-induced MAPK/ERK and Elk-1 activation *in vivo* depends on dopaminergic transmission. *Eur. J. Neurosci.* **14**, 342–352 (2001).
26. Impey, S., Obrietan, K. & Storm, D.R. Making new connections: role of ERK/MAP kinase signaling in neuronal plasticity. *Neuron* **23**, 11–14 (1999).
27. Kandel, E.R. The molecular biology of memory: cAMP, PKA, CRE, CREB-1, CREB-2, and CPEB. *Mol. Brain* **5**, 14 (2012).
28. Villeda, S.A. *et al.* Young blood reverses age-related impairments in cognitive function and synaptic plasticity in mice. *Nat. Med.* **20**, 659–663 (2014).
29. Fusco, S. *et al.* A role for neuronal cAMP responsive-element binding (CREB)-1 in brain responses to calorie restriction. *Proc. Natl. Acad. Sci. USA* **109**, 621–626 (2012).
30. Saura, C.A. & Valero, J. The role of CREB signaling in Alzheimer's disease and other cognitive disorders. *Rev. Neurosci.* **22**, 153–169 (2011).
31. West, A.E. *et al.* Calcium regulation of neuronal gene expression. *Proc. Natl. Acad. Sci. USA* **98**, 11024–11031 (2001).
32. Das, C. *et al.* Binding of the histone chaperone ASF1 to the CBP bromodomain promotes histone acetylation. *Proc. Natl. Acad. Sci. USA* **111**, E1072–E1081 (2014).
33. Vecsey, C.G. *et al.* Histone deacetylase inhibitors enhance memory and synaptic plasticity via CREB:CBP-dependent transcriptional activation. *J. Neurosci.* **27**, 6128–6140 (2007).
34. Shieh, P.B., Hu, S.C., Bobb, K., Timmusk, T. & Ghosh, A. Identification of a signaling pathway involved in calcium regulation of *BDNF* expression. *Neuron* **20**, 727–740 (1998).
35. Gao, H. *et al.* Long-term dietary α-linolenic acid supplement alleviates cognitive impairment correlate with activating hippocampal CREB signaling in natural aging rats. *Mol. Neurobiol.* **53**, 4772–4786 (2016)
36. Gräff, J. & Tsai, L.H. Histone acetylation: molecular mnemonics on the chromatin. *Nat. Rev. Neurosci.* **14**, 97–111 (2013).
37. Peleg, S. *et al.* Altered histone acetylation is associated with age-dependent memory impairment in mice. *Science* **328**, 753–756 (2010).
38. Bilkei-Gorzo, A. *et al.* Early age-related cognitive impairment in mice lacking cannabinoid CB1 receptors. *Proc. Natl. Acad. Sci. USA* **102**, 15670–15675 (2005).
39. Albayram, O. *et al.* Role of CB1 cannabinoid receptors on GABAergic neurons in brain aging. *Proc. Natl. Acad. Sci. USA* **108**, 11256–11261 (2011).
40. Piyanova, A. *et al.* Loss of CB1 receptors leads to decreased cathepsin D levels and accelerated lipofuscin accumulation in the hippocampus. *Mech. Ageing Dev.* **134**, 391–399 (2013).
41. Monory, K. *et al.* The endocannabinoid system controls key epileptogenic circuits in the hippocampus. *Neuron* **51**, 455–466 (2006).
42. Fischer, A., Sananbenesi, F., Wang, X., Dobbin, M. & Tsai, L.H. Recovery of learning and memory is associated with chromatin remodelling. *Nature* **447**, 178–182 (2007).
43. Day, J.J. & Sweatt, J.D. Epigenetic treatments for cognitive impairments. *Neuropsychopharmacology* **37**, 247–260 (2012).


© 2017 Nature America, Inc., part of Springer Nature. All rights reserved.

## ONLINE METHODS

**Animals.** C57BL/6J mice were bred at the House of Experimental Therapy, University of Bonn or obtained from a commercial breeder (Janvier, France). In the latter case, animals were habituated to the animal facility for 2 weeks before the experiments. Experiments with *Cb1* knockout mice were carried out with male $Cb1^{+/+}$ and $Cb1^{-/-}$ littermates aged 12 months[44]. Glutamatergic neuron–specific *Cb1* knockouts were obtained by crossing $Cb1^{fl/fl}$ mice[41] with a *Neurod6-Cre* deletion strain. Both the constitutive and conditional knockout lines were on a congenic C57BL6/J background. All experiments followed the guidelines of European Community's Directive 86/609/EEC and the German Animal Protection Law regulating animal research. They were approved by LANUV NRW.

**Power analysis.** Power analyses indicated an 80% probability of detecting a 30% change for animal experiments. In immunoblots, we had sufficient power to detect a 45% change, in the real-time PCR studies a 50% change, in the histological analysis, 25% differences and, in Illumina gene expression profiling or ChIP analysis, a 50% difference between groups with 80% probability.

**Drug treatment.** Male C57BL/6J mice aged 2 months (young), 12 months (mature) and 18 months (old) were chronically treated with THC (3 mg per kg bodyweight per day)[45,46] or vehicle (ethanol:cremophor:saline, 1:1:18)[47–49] through subcutaneously implanted osmotic minipumps (Alzet, CA, USA) for 28 d. The animals were randomly selected for the treatment groups. To test the effect of the histone acetylation blockade, male C57BL/6J mice aged 12 months were purchased from Janvier (France). Half of the animals received vehicle and the other half received a THC dose of 3 mg per kg bodyweight per day through osmotic minipumps as described above. During THC treatment (28 d), the animals received daily either vehicle or 5 mg per kg bodyweight anacardic acid intraperitoneally. For solubilization, we used DMSO:Tween-20: saline at a ratio of 2:5:93.

**Behavioral testing.** The novel object location recognition test was performed in a sound-isolated, dimly illuminated room in an open-field box (44 cm × 44 cm). The floor was covered with sawdust (1 cm deep, used and saturated with the odor of the animals). The habituation period consisted of a daily 5-min period of free exploration in the arena containing three objects (plastic balls, 15 mm in diameter) for 3 d. On the test day, the animals were allowed to explore three identical objects (Lego pieces with different colors, roughly 2 × 2 cm) placed into the area in a fixed location for 6 min, and the time spent on inspection of the individual objects was recorded (Noldus Ethovision XT). Thirty minutes later, the animals were placed back into the box, where one object was placed into a new location. The animals were left to explore for an additional 3 min. The time spent with investigations was recorded, and the preference ratio for the moved object was calculated as follows: preference = $T_a/(T_a + T_b + T_c) \times 100$; $T$, time spent with investigation; $T_a$, the object that is moved in the second trial; $T_b$ and $T_c$, the objects that remained in their original positions. Novelty preference was calculated as follows: $(P_{t2} - P_{t1})/P_{t1} \times 100$; $P$, the preference of the mouse; t1, trial one; t2, trial two.

Long-term memory was tested using a modified form of the partner recognition test 42 d after the minipump implantation. The test was performed in the same arenas and after the same habituation as described for the novel object location recognition test. In the first trial, the arenas held both a metal grid cage only containing a mouse (of the same age and sex as the test animal but from a different cage) and one other object (of a similar size and form as the metal grid cage) in the opposing corner, placed 6–7 cm from the walls. The location and activity of the test mouse were recorded and analyzed by the EthoVision tracking system (Noldus) for 15 min. In the next session, after 24 h, the object was replaced with another grid cage containing a new partner and the activity of the test mouse was recorded again for 5 min. Recognition of the previously seen partner was defined by a novelty preference, i.e., a significantly longer period spent investigating the new partner in the second trial. Novelty preference was calculated as $T_a/(T_a + T_b) \times 100$; $T_a$ is the time spent with the novel partner; $T_b$ is the time spent with the previous partner.

Spatial learning and memory were assessed in the MWM task as described[39,50,51]. In the acquisition phase of the MWM test, the animals were tested for four consecutive sessions daily over 5 d. The hidden platform remained at a fixed spatial location for the entire acquisition period. The mice started from the same position at days 1 and 2 and from variable positions in the following trials. Long-term spatial memory was assessed at day 6, when the platform was removed and the time spent in the platform-associated quadrant was measured. We assessed the flexibility of spatial memory by placing the platform in a new location (reversal phase) between days 7 and 9. Animals that did not move (floater) or just circled in close vicinity to the wall (wall-hangers) were excluded from the analysis and further tests. The criteria were pre-established. The investigator was blinded to genotype or treatment, but the difference between the age groups was clearly visible. Recording and analysis of behavior were carried out by automated systems (Videomot, TSE-Systems).

**Tissue preparation.** Animals were euthanized by $CO_2$ inhalation 5 d after the last behavioral test, decapitated and their brains were isolated. Brains were snap frozen in dry-ice-cooled isopentane and stored at −80 °C until further processing. For immunoblot and gene expression experiments, hippocampi were isolated from the frozen brains in a cryostat (Leica CM 3050; Leica Microsystems, Heidelberg, Germany) using the punch technique[39,52]. For histology, brain areas containing the dorsal region of the hippocampus were serially cut into 18-µm coronal slices ($n$ = 8 per mouse) in a cryostat (Leica CM 3050; Leica Microsystems, Heidelberg, Germany) and mounted onto silanized glass slides.

**Gene expression profiling.** Whole hippocampi were lysed in TRIzol (Life Technologies), and total RNA was extracted according to the manufacturer's protocol. The quality of the RNA was assessed by measuring the ratio of the absorbance at 260 nm and 280 nm using a Nanodrop 2000 Spectrometer (Thermo Scientific), as well as by visualization of the integrity of the 28S and 18S bands on an agarose gel. Prior to array-based gene expression profiling, total RNA was further purified using the MinElute Reaction Cleanup Kit (Qiagen). Biotin-labeled cRNA was generated using the TargetAmp Nano-g Biotin-aRNA Labeling Kit for the Illumina System (Epicentre). Biotin-labeled cRNA (1.5 µg) was hybridized to MouseWG-6 v2.0 BeadChips (Illumina) and scanned on an Illumina HiScanSQ system. Raw intensity microarray data were processed using GenomeStudio V2011.1 (Illumina). Subsequent analyses were performed using Partek Genomics Suite V6.6 (PGS) (Partek). Non-normalized data were imported from GenomeStudio using the default PGS report builder. After quantile normalization in PGS, variable transcripts, as well as significantly differentially expressed transcripts, were calculated by employing a two-way ANOVA model. Variable genes were defined by an unadjusted $P$ value of <0.05, and significantly differentially expressed transcripts were defined by an unadjusted $P$ value of <0.05 and a fold change of ±2. Variable genes were further analyzed by unsupervised hierarchical clustering using PGS default settings visualizing condition-specific similar or differential gene expression. The statistical significance of the correlations between two or more groups was determined by ANOVA modeling, and the corresponding $P$ value was computed. $P$ values of <0.05 were defined as significant. Statistical analysis was performed using Partek Genomics Suite.

To validate the previous analysis that was based on the ANOVA model, we additionally performed a weighted gene coexpression network analysis (WGCNA). We used WGCNA to identify specific signatures that can be associated with one or more conditions. The WGCNA R package (http://labs.genetics.ucla.edu/)[53] was used for the analysis. The standard parameters were altered to a power of 19 and a minModuleSize of 30, resulting in 10 modules using 1,721 variable genes. For each module, the eigengene (ME) corresponding to the first principal component of a given module was calculated. The network for each module of interest was generated using the '1-TOMsimilarityFromExpr' function of the WGCNA R package. Each module was associated with a trait having the highest Pearson correlation coefficient. Gene-to-module association can be found in **Supplementary Table 1**. Module-to-gene ontology enrichment can be found in **Supplementary Table 2**. It should be noted that our analysis strategy did not use FDR-adjusted $P$ values. We used the gene sets passing a fold change cutoff and the unadjusted $P$ value to determine biological processes by GOEA followed by network visualization of significantly enriched GO terms. From our experience, this analysis requires the use of a sufficient number of genes;

© 2017 Nature America, Inc., part of Springer Nature. All rights reserved.

otherwise, calling GO terms becomes arbitrary. In this case, where the approach using the FDR-corrected *P* value did not result in a sufficient gene number, we have changed our model by using the unadjusted *P* value. Owing to the difficult sample preparation and a late time point after intervention, we were anticipating high variance of signals and low effect sizes. These experimental limitations require a less stringent cutoff for defining genes for further downstream analysis (either computationally or experimentally). We are aware that this represents a compromise. The transcriptome analysis defined candidate genes that were then PCR validated (for an example, see **Fig. 3**). In retrospect, the successful PCR validation justified the use of this approach.

Real-time RT–PCR mRNA expression analysis was performed using total RNA, which was isolated from the frozen hippocampi of mice ($n$ = 6–8) and reverse transcribed to cDNA as reported previously[39], using custom TaqMan Gene Expression Assays (Applied Biosystems, Darmstadt, Germany) Mm01334042_m1 for BDNF, Mm00438023_m1 for caspase-1, Mm01192932_g1 for Ctgf, Mm00502002_m1 for Kl and Mm00443267_m1 for Ttr. 3-Phosphate dehydrogenase (GAPDH; Mm01334042_m1) was used as an endogenous control to standardize the amount of target cDNA. For the longitudinal study of the expression of two splice variants of *Kl*, mKlotho and sKlotho, qPCR was performed as described[54] on a LightCycler 480 II (Roche) PCR machine using LightCycler 480 SYBR Green I master mix (Roche). A two-step PCR reaction was carried out as follows: one cycle at 98 °C for 2 min followed by 40 cycles of 95 °C for 5 s and 58 °C for 30 s. Samples were run as triplicates. All samples were normalized to m36B4, which was used as a reference gene. Gene-specific primers are listed in **Supplementary Table 3**. Relative quantitative gene expression was calculated with the $2^{-\Delta\Delta CT}$ method[55]. Mean $2^{-\Delta CT}$ values of vehicle-treated animals of both ages were chosen as reference samples and subtracted from $2^{-\Delta CT}$ of the other groups ($\Delta\Delta C_T$).

**Immunoblots.** Frozen hippocampi were lysed in 1% SDS buffer (Sigma-Aldrich, Munich, Germany) containing protease and phosphatase inhibitors (Complete Mini, Roche; PhosStop, Roche), sonicated and clarified by centrifugation (9,500*g* for 10 min). Protein concentrations were determined using a BCA Protein Assay Kit (Pierce). Equal amounts of protein were run on NuPAGE Bis-Tris 4–12% gradient gels (Invitrogen, Carlsbad, CA). The proteins were subsequently blotted onto PVDF membranes using the iBlot Dry Blotting System (Invitrogen, Carlsbad, CA). The blots were incubated with primary antibodies to Akt (1:1,000; Cell Signaling, 9272), phospho-Akt Ser473 (1:1,000; Cell Signaling, 9272S), ERK1/2 (1:1,000; Sigma, M3807), phospho-ERK (1:1,000; Sigma, M9692), CREB (1:1,000; Abcam, ab32515), phospho-CREB Ser133 (1:1,000; Abcam, ab10564), PSD95 (1:200; Abcam, ab18258), synapsin I (1:200; Abcam, ab64581), synaptophysin (1:200; Millipore, 04-1019), histone H3 (1:500; Abcam, ab10799), histone H4 (1:500; Abcam, ab16483), histone H2A (1:500; Abcam, ab18255), histone H3 acetyl K9 (1:500; Abcam, ab4441), H3 trimethylated K9 (1:500; Abcam, ab8898), H4 acetyl K12 (1:500; Abcam, ab46983), H2A acetyl K5 (1:500; Abcam, ab1764), and with a Gapdh (1:5,000; Abcam, ab9484) or a β-actin antibody (1:10,000; Sigma, A5441-2ML) to ensure equal loading. Validation of the antibodies was performed by the manufacturer. Please refer to their websites for further information. The blots were then incubated with peroxidase-conjugated secondary antibodies. Signals were detected using chemiluminescent substrate for the peroxidase (ECL, Pierce). Images were created either using the ChemiDoc Imaging System (Bio-Rad) or by covering the membranes by ECL substrate (Pierce), covered with high-performance autoradiography film (Amersham Hyperfilm MP, GE Healthcare, Buckinghamshire, UK) and developed using a CP 1000 AGFA Healthcare N.V. film developer. The films were then scanned using an Epson Perfection 4990 scanner and analyzed using ImageJ software. Images from the ChemiDoc System were quantified using ImageLab software (Bio-Rad).

**Immunofluorescence.** Slides were placed in 0.1 M (pH 7.3) PBS for 5 min to thaw after storage at −80 °C, followed by post-fixation in 4% paraformaldehyde dissolved in PBS for 30 min. After a 5-min wash in PBS, slides were permeabilized using 0.2% Triton X-100 for 20 min and then washed again for 5 min in PBS. Blocking of unspecific binding sites was done with PBS containing 5% donkey serum albumin for 10 min followed by another PBS wash for 5 min. The slices were first kept in 4 °C for 48 h in rabbit anti–synapsin I solution (Abcam, ab64581; diluted 1:250 in PBS), 48 h in rabbit anti-Klotho antibody solution (Thermo Fisher, PA5-21078; diluted 1:400 in 3% BSA in PBS), sheep anti-prealbumin antibody solution (Abcam, ab9015; diluted 1:500 in 0.3% BSA in PBS), AF488-coupled mouse anti-NeuN antibody (Millipore, MAB377X; diluted 1:200 in 0.3% BSA in PBS), rabbit anti-Iba1 antibody solution (Wako, 016-20001: diluted 1:200), rabbit anti-VGAT or VGLUT1 (both donated by B. Schütz, University of Marburg; diluted 1:1,000 and 1:10,000, respectively). Afterwards, the slides were rinsed three times for 10 min in PBS before incubation with goat anti-rabbit Cy3-conjugated secondary antibody (Life Technologies, A10520; diluted 1:500 in 0.3% BSA in PBS) for synapsin I, donkey anti-rabbit AF647-conjugated secondary antibody (Invitrogen, A31573; diluted 1:2,000 in 0.3% BSA in PBS) for Klotho, donkey anti-rabbit AF488-conjugated secondary antibody (Life Technologies, A21206; diluted 1:2,000 in 0.3% BSA in PBS) for Iba1, donkey anti-sheep AF647-conjugated (Jackson Immuno, 713-175-147; diluted 1:2,000 in 0.3% BSA in PBS) or AF488-conjugated (Invitrogen, A11015, diluted 1:1,000 in 0.3% BSA in PBS) for transthyretin secondary antibody in a humid chamber for 2 h in the dark. After staining, the sections were again rinsed three times for 5 min and were mounted with DAPI-containing Fluoromount-G (SouthernBiotech, USA) and covered. The NeuN co-stained slices were first dehydrated with an increasing concentration of ethanol and xylol, mounted with Rotihisto II (Carl Roth, Germany) and covered. For quantitative analysis of synapsin I, Klotho or transthyretin immunoreactivity, fluorescence images were acquired using a Zeiss Axiovert 200M fluorescent microscope (Carl Zeiss Microimaging, Oberkochen, Germany) with a 20×, 0.8 NA lens. Immunoreactivities were analyzed with ImageJ software (ImageJ 1.42q, NIH, USA) using the integrated density technique[56]. For quantitative analysis of staining intensities, six pictures per animal were taken. Each group consisted of three animals. The images were converted to 8-bit grayscale using ImageJ software and signal intensities (calculated as mean signal intensity within the region of interest (ROI; pyramidal cell layer in the CA3 region of the hippocampus)) minus the signal intensity outside but adjacent to the ROI (stratum radiatum in the CA3 region) were calculated. For quantitative analysis of the density of VGAT- or VGLUT1-positive puncta around CA3 pyamidal neurons, fluorescence images were acquired using a Zeiss Axiovert 200M fluorescent microscope (Carl Zeiss Microimaging, Oberkochen, Germany) with a 63×, 1.3 NA oil-immersion lens. Density was determined as the number of puncta divided by the area of the CA3 neuron with ImageJ software (ImageJ 1.42q, NIH, USA). For testing colocalization, the Leica LSM SP8 confocal microscope was used.

**Golgi staining.** For Golgi staining, a kit from FD NeuroTechnologies (USA) was used following the instructions of the manufacturer. Microphotographs from dendrites of selected neurons were taken using a Zeiss Axiovert 200M fluorescent microscope (Carl Zeiss Microimaging, Oberkochen, Germany) with a 63×, 1.3 NA oil-immersion lens. Density was determined as the number of spines on the terminal 50-µm sequence of a dendrite divided by the length of the dendrite as determined with ImageJ software (ImageJ 1.42q, NIH, USA).

**Chromatin immunoprecipitation.** To test whether the expression of BDNF and Klotho was affected by histone modification, we applied chromatin immunoprecipitation analysis using the Diagenode LowCell ChIP Kit following the instructions of the manufacturer. Briefly, mice were decapitated, and their hippocampi were isolated and fixed overnight in 4% paraformaldehyde. After washing, the hippocampi were lysed and chromatin was sheared by sonication (Bioruptor Plus, Diagenode). Sheared chromatin was incubated with magnetic beads covered with antibodies for histone modifications (AcH3K9 and H3). Next, the beads were removed, washed and the attached DNA was purified. Histone modifications of the *Bdnf* or *Kl* promoter loci were assessed by SYBR Green quantitative PCR. Primer sequences are shown in **Supplementary Table 1**.

**Statistics.** Data analyzed were all numeric. Distribution analysis was done with the data from spine and axon terminal densities, but not with other data with low case numbers. Variances were compared by Bartlett statistic to decide whether parametric tests were applicable. In the MWM test, the latency to reach the platform and the speed of the animals were analyzed using two-way ANOVA (between factor, group; within factor, trial) followed

© 2017 Nature America, Inc., part of Springer Nature. All rights reserved.


doi:10.1038/nm.4311

by Bonferroni´s *t*-test. Time to reach the visible platform or time spent in the target sector during the probe trial was analyzed using one-way ANOVA followed by Bonferroni's *t*-test. Data from the partner-recognition test were analyzed using one-way ANOVA. Novel object location recognition test results were analyzed using one-way ANOVA (separately to the time points) followed by Bonferroni's *t*-test. To analyze synapsin I staining intensity and levels of synaptic proteins determined by immunoblotting, results were analyzed using one-way ANOVA followed by Bonferroni's *t*-test. For the analysis of VGAT, VGLUT1 and dendrite spine densities, Kruskal–Wallis ANOVA followed by Dunn's test was used. Gene expression (Illumina, RT–PCR) was analyzed using one-way ANOVA followed by Bonferroni's *t*-test. Staining intensity of Ttr and Klotho was analyzed using one-way ANOVA followed by Bonferroni's *t*-test. Brain-region-specific expression of Klotho and transthyretin was analyzed using the Mann–Whitney test. Immunoblot results for protein phosphorylation and histone acetylation were tested using one-way ANOVA followed by Bonferroni's *t*-test. Results of the ChIP analysis were analyzed using the Student's unpaired two-sided *t*-test.

**Data availability.** The Gene Expression Omnibus (GEO) accession number of the expression profiling data is GSE57823.


44. Zimmer, A., Zimmer, A.M., Hohmann, A.G., Herkenham, M. & Bonner, T.I. Increased mortality, hypoactivity, and hypoalgesia in cannabinoid CB1 receptor knockout mice. *Proc. Natl. Acad. Sci. USA* **96**, 5780–5785 (1999).
45. Lastres-Becker, I., Molina-Holgado, F., Ramos, J.A., Mechoulam, R. & Fernández-Ruiz, J. Cannabinoids provide neuroprotection against 6-hydroxydopamine toxicity *in vivo* and *in vitro*: relevance to Parkinson's disease. *Neurobiol. Dis.* **19**, 96–107 (2005).
46. Varvel, S.A. *et al*. Interactions between THC and cannabidiol in mouse models of cannabinoid activity. *Psychopharmacology (Berl.)* **186**, 226–234 (2006).
47. Marchalant, Y., Brothers, H.M. & Wenk, G.L. Cannabinoid agonist WIN-55,212-2 partially restores neurogenesis in the aged rat brain. *Mol. Psychiatry* **14**, 1068–1069 (2009).
48. Galve-Roperh, I. *et al*. Anti-tumoral action of cannabinoids: involvement of sustained ceramide accumulation and extracellular signal–regulated kinase activation. *Nat. Med.* **6**, 313–319 (2000).
49. Sánchez, I., Mahlke, C. & Yuan, J. Pivotal role of oligomerization in expanded polyglutamine neurodegenerative disorders. *Nature* **421**, 373–379 (2003).
50. Barnes, C.A., Suster, M.S., Shen, J. & McNaughton, B.L. Multistability of cognitive maps in the hippocampus of old rats. *Nature* **388**, 272–275 (1997).
51. Sanchez-Mejia, R.O. *et al*. Phospholipase $A_2$ reduction ameliorates cognitive deficits in a mouse model of Alzheimer's disease. *Nat. Neurosci.* **11**, 1311–1318 (2008).
52. Cannich, A. *et al*. CB1 cannabinoid receptors modulate kinase and phosphatase activity during extinction of conditioned fear in mice. *Learn. Mem.* **11**, 625–632 (2004).
53. Langfelder, P. & Horvath, S. WGCNA: an R package for weighted correlation network analysis. *BMC Bioinformatics* **9**, 559 (2008).
54. Massó, A. *et al*. Secreted and transmembrane αklotho isoforms have different spatio-temporal profiles in the brain during aging and Alzheimer's disease progression. *PLoS One* **10**, e0143623 (2015).
55. Livak, K.J. & Schmittgen, T.D. Analysis of relative gene expression data using real-time quantitative PCR and the $2^{-\Delta\Delta CT}$ method. *Methods* **25**, 402–408 (2001).
56. Miró, X. *et al*. Haploinsufficiency of the murine Polycomb gene *Suz12* results in diverse malformations of the brain and neural tube. *Dis. Model. Mech.* **2**, 412–418 (2009).


© 2017 Nature America, Inc., part of Springer Nature. All rights reserved.